Journal of Power Sources 415 (2019) 1–7

Contents lists available at ScienceDirect

Journal of Power Sources

journal homepage: www.elsevier.com/locate/jpowsour

Massively manufactured paper-based all-solid-state flexible micro-supercapacitors with sprayable MXene conductive inks

Haichao Huang[a], Xiang Chu[a], Hai Su[a], Haitao Zhang[a,*], Yanting Xie[a], Wen Deng[a], Ningjun Chen[a], Fangyan Liu[a], Hepeng Zhang[a], Bingni Gu[a], Weili Deng[a], Weiqing Yang[a,b,**]

[a] Key Laboratory of Advanced Technologies of Materials (Ministry of Education), School of Materials Science and Engineering, Southwest Jiaotong University, Chengdu, 610031, China

[b] State Key Laboratory of Traction Power, Southwest Jiaotong University, Chengdu, 610031, China

HIGHLIGHTS

- It can easily achieve large-scale manufacturing and integration.
- $Ti_3C_2T_x$ MXene acts as both the active material and current collection.
- The configurations are optimized to obtain the best electrochemical performance.
- Flexible paper-based micro-supercapacitors with excellent performance are obtained.

GRAPHICAL ABSTRACT

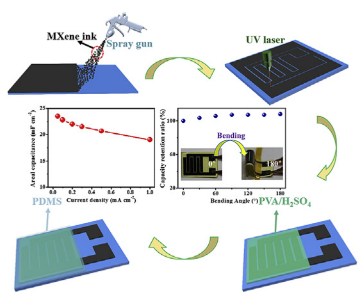

ARTICLE INFO

Keywords:
Paper-based microelectronics
Flexible micro-supercapacitors
Spray coating
All-solid-state
High areal specific capacitance

ABSTRACT

Flexible micro-supercapacitors (FMSCs) are promising candidates for portable and on-chip energy storage due to their miniaturization, lightweight and high-security. Till now, FMSCs still suffer from several limitations, such as complex fabricating process, low areal energy storage, and short cycling lifetime, badly inhibiting its wider on-chip integrated applications. Here, we directly employ an easy-processing spray coating of the $Ti_3C_2T_x$ MXene conductive inks to massively fabricate the paper-based all-solid-state FMSCs. Instead of traditional noble metals Au as current collector, the sprayable and highly conductive $Ti_3C_2T_x$ MXene interdigitated electrodes serve the dual function of the active materials and current collection. Based on it, we develop an all-solid-state FMSC by employing polyvinyl alcohol & H_2SO_4 gel-like solid-state electrolyte and self-flowed polydimethylsiloxane encapsulated layer. With further optimizing the geometric configurations of interdigitated electrodes, the as-prepared FMSCs exhibit high areal capacitance of 23.4 mF cm^{-2} and excellent rate-capability of 81.4%. Moreover, these paper-based FMSCs also demonstrate outstanding cyclic capability of 92.4% capacitance retention after 5000 cycles, along with remarkable flexibility. Consequently, we believe that this innovative strategy will open new avenues for easily and largely fabricating various FMSCs to further promote the integration of portable and on-chip energy storage systems.

* Corresponding author.

** Corresponding author. Key Laboratory of Advanced Technologies of Materials (Ministry of Education), School of Materials Science and Engineering, Southwest Jiaotong University, Chengdu, 610031, China.

E-mail addresses: haitaozhang@swjtu.edu.cn (H. Zhang), wqyang@swjtu.edu.cn (W. Yang).

https://doi.org/10.1016/j.jpowsour.2019.01.044
Received 23 October 2018; Received in revised form 4 January 2019; Accepted 15 January 2019
0378-7753/

1. Introduction

The continuous advancement of portable and wearable electronic devices (such as mobile phones, digital cameras, and tablet personal computers) requires the storage and conversion devices to be small, flexible, lightweight, capability of curling and even wearable [1–3]. As a promising storage energy device, supercapacitors have attracted lots of attention in recent years, due to their high charge-discharge rate, high power density and excellent cycling stability with minimal maintenance [4–6]. To meet the demand of lightweight, small size and flexibility for portable electronic devices, all-solid-state flexible micro-supercapacitors (FMSCs) are considered as the most potential candidate [7,8]. In recent years, some breakthroughs like high temperature flexible capacitor [9], shape memory flexible supercapacitor [10] have been made in FMSCs. However, there still remain some challenges in FMSCs, such as high processing costs, complex architecture, low areal energy storage capability, and limited cycling lifetime, which limit their practical application and integration [11].

In general, some soft substrates are always indispensable for FMSCs. Paper has been considered as an alternative substrate due to its light weight, excellent flexibility, and lower cost than other flexible substrates [12,13], such as polyethylene terephthalate (PET), polypropylene (PP), and other elastic materials. Apart from that, paper is also much more environmentally friendly. Furthermore, when it comes to the configuration of flexible FMSCs, researchers are inclined to adopt the in-plane interdigitated form [14,15]. It's because that the interdigitated form can not only be free from membranes, but also be beneficial for the rapid ionic diffusion and easy integration with other related on-chip microelectronics.

Besides, since the intrinsic properties of electrode materials play the most important role in affecting the performance of FMSCs, it is critical to find one material with outstanding conductivity as well as excellent electrochemical performance. Recently, a class of 2D metal carbides and nitrides which named MXene (of the formula $M_{n+1}X_nT_x$, where M is a transition metal, X is C and/or N, and T_x represents surface functionalization, n = 1, 2, or 3) has attracted increased attention due to its outstanding electrical conductivity, high mechanical stability and excellent electrochemical performance [16,17]. To data, more than 20 MXenes have been discovered and synthesized. Among these MXenes, $Ti_3C_2T_x$ is the most widely researched one for energy storage application, which exhibited much higher volumetric capacitances than most previously reported materials [18], such as carbon nanotubes [19], carbide-derived carbon [20], grapheme [21], porous carbons [22]. Compared to other electrode materials like graphene, $Ti_3C_2T_x$ MXene is hydrophilic due to the rich hydrophilic reactive functional groups on the MXene nanosheets, so that it can form a stable aqueous dispersion without adding surfactant or polymer. What's more, $Ti_3C_2T_x$ possesses high electronic conductivity up to 6500 S cm^{-1}, evidently enabling it to act as both the active material and the current collector for the FMSCs [23].

In this work, we report an easy-processing spray coating approach to massively fabricate the paper-based all-solid-state FMSCs with sprayable MXene conductive inks. The $Ti_3C_2T_x$ paper electrodes for the in-plane FMSCs were obtained via facile spraying and direct cold laser machining selectively using a 355 nm ultraviolet laser. On the one hand, the prominent feature of paper-based all-solid-state FMSCs we designed is that no precious metals are used throughout the whole manufacturing process which immensely outs the cost, while precious metals are present at most reported paper-based FMSCs to support electron transmission [24,25]. On the other hand, since the configuration of FMSCs plays an essential role in affecting the ion diffusion and transfer, the interdigitated width and distance have been optimized systematically. Except for the above two advantages, the used cold light processing can effectively avoid the intrinsically burning damage of paper electrode edge from the traditional hot 1064 nm infrared laser. This burning damage of edge will obstruct the electrolyte ion transport and then naturally reduce the electrochemical performance of FMSC. Consequently, the paper-based FMSC demonstrated a collection of outstanding performance, including high areal specific capacitance (23.4 mF cm^{-2}), remarkable flexibility, and excellent capacitance retention (92.5% retain ability after 5000 cycles at 1 mA cm^{-2}), and highly integrated ability. Herein reported simply sprayable and highly conductive paper-based electrodes is expected to pave a novel way for massive manufacture of all-solid-state FMSCs with remarkable mechanical and electrochemical properties, which can further promote the integration of FMSCs in portable and on-chip microelectronics.

2. Experimental section

2.1. Synthesis of $Ti_3C_2T_x$ MXene inks

Multi-layer $Ti_3C_2T_x$ MXene powder was synthesized according to our previous work [35]. Typically, multi-layer $Ti_3C_2T_x$ (m-$Ti_3C_2T_x$) was firstly prepared via a chemical etching method by hydrochloric acid (HCl) and lithium fluoride (LiF). Then, to obtain the few-layer $Ti_3C_2T_x$ (f-$Ti_3C_2T_x$), 0.8 g m-$Ti_3C_2T_x$ were mixed with 100 ml deionized water (DI water) and kept under ultrasonic for 1 h. After that, the dark green supernatant was collected by centrifugation at 3500 rpm for 1 h, which was the $Ti_3C_2T_x$ MXene ink we need.

2.2. Synthesis of $Ti_3C_2T_x$ paper electrode

The $Ti_3C_2T_x$ paper electrode was prepared via spraying and UV laser cutting. Firstly, 20 mL $Ti_3C_2T_x$ MXene inks were sprayed on the PET coated paper with an area of 12*8 cm^2 under the N_2 flow of 0.15 MPa, followed by drying at room temperature for 24 h. Then, the interdigitated electrodes with different width w and distance d of interdigitated fingers were prepared through ultraviolet laser marking technology (UV-3S, China).

2.3. Synthesis of gel electrolyte

First, 8 g concentrated H_2SO_4 with a mass ratio of 98% was slowly added into 80 mL DI water. Then, 8 g polyvinyl alcohol (PVA) (1799 type) were added into the H_2SO_4 aqueous solution after the solution cooled down to room temperature. The above-obtained solution was stirred for 1 h in a water bath of 80 °C, followed by standing for 1 h until the solution cooled down to room temperature.

2.4. Fabrication of paper-based flexible solid-state micro-supercapacitor (FMSCs)

The manufacturing process of flexible solid-state micro-supercapacitor (FMSCs) was shown as Fig. 1. The as-prepared paper-based MXene electrodes was poured with PVA/H_2SO_4 gel electrolyte, following by standing for 40 min to make the gel electrolyte semi-solidified. After that polydimethylsiloxane (PDMS) module glue was carefully dropped onto the electrodes, and then the device was left in air for 24 h at room temperature to complete the package. When the PDMS module glue was curing, flexible solid-state FMSCs were successfully prepared.

2.5. Characterizations

XRD patterns were measured using a powder diffractometer (PANalytical X'Pert Powder diffractometer, Holland) with Cu Ka radiation at a step scan of 0.02° over a 2θ range of 5–50°. The morphology of the MXene sheets and electrodes was imaged using a SEM (FEI QUANTA FEG 250, American), which was also used to obtain the conduct elemental analysis via Energy Dispersive X-ray (EDX) Spectroscopy. Raman spectra were obtained from a RM2000 microscopic confocal Raman spectrometer with a 514 nm Ar ions laser beam.

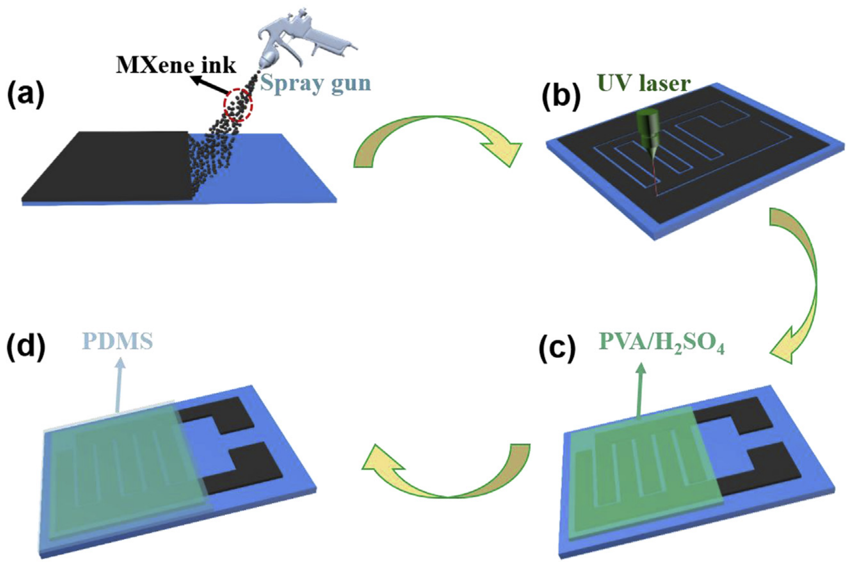

Fig. 1. Schematic illustrating the fabrication process of paper-based all-solid-state FMSCs with MXenes as both active materials and current collectors. (a) $Ti_3C_2T_x$ MXene ink was sprayed on the PET coated paper with an area of 12*8 cm^2. (b) The pattern of electrode was carved through UV laser cutting. (c) Poured the PVA/H_2SO_4 gel electrolyte on the interdigitated part of the electrode. (d) PDMS module glue was carefully dropped onto the electrodes.

2.6. Electrochemical measurements

All the electrochemical measurements were conducted with a CHI 660E electrochemical workstation (Chenhua, Shanghai, China). The cyclic voltammetry (CV) tests were performed at a scan rate ranging from 5 to 100 mV s^{-1} in the potential window of 0–0.6 V. Galvanostatic charge/discharge (GCD) was carried out at the current density of 0.05, 0.1, 0.2, 0.3, 0.5 and 1 mA cm^{-2} in the same potential window. Electrochemical impedance spectroscopy (EIS) was performed at open circuit potential and frequencies ranging from 10 KHz to 0.1 Hz. In addition, an Arbin MSTAT4 multi-channel galvanostat/potentiostat instrument (Arbin, USA) was used to measure the cycling stability. The areal capacitance (C_A), the volumetric energy density (E_V), and the volumetric power density (P_V) was calculated as following:

$$C_A = I_s \cdot \Delta t \,/\, (\Delta U \cdot S)\ (\text{mF cm}^{-2}) \tag{1}$$

$$E_V = C_A \cdot V^2 \,/\, (2 \cdot 3.6 \cdot h)\ (\text{mWh cm}^{-3}) \tag{2}$$

$$P_V = 3.6\ E_V \,/\Delta t\ (\text{mW cm}^{-3}) \tag{3}$$

Where I_s is the charge-discharge current density based on the areal parameter, Δt is GCD discharge time after the *Voltage drop*, ΔU is potential window after the *Voltage drop*, S is the efficient area of the electrodes, h is the thickness of the coated MXene layer and V is potential.

3. Results and discussion

The fabrication process of paper-based all-solid-state FMSCs is shown in Fig. 1. A spray-coating method was employed to deposit highly conductive $Ti_3C_2T_x$ flakes on a flexible substrate of polyethylene terephthalate (PET) coated paper (Fig. 1a and Movie S1, Supporting Information). Importantly, no precious metal (gold, platinum, or other alloys) was used in our paper-based FMSCs since the MXene with excellent conductivity of 1025 S cm^{-2} can simultaneously serve as both the active material and the current collector, which greatly reduces the manufacturing cost of paper-based FMSCs. Then the interdigitated pattern with different width (w) and distance (d) was obtained via direct ultraviolet laser cutting (Fig. 1b). In practice, the ultraviolet laser (355 nm) carving can guarantee only minor damage on the edge of the interdigitated electrodes. After the interdigitated electrodes were fabricated, PVA/H_2SO_4 gel electrolyte was utilized as the solid-state electrolyte (Fig. 1c). Finally, the whole flexible all-solid-state paper-based FMSCs were obtained after the encapsulation with PDMS (Fig. 1d). Excitedly, the whole all-solid-state paper-based FMSCs can be easily and massively manufactured using low-cost and environmentally friendly approaches.

Supplementary video related to this article can be found at https://doi.org/10.1016/j.jpowsour.2019.01.044.

$Ti_3C_2T_x$ MXene was prepared via a mild method by hydrochloric acid (HCl) and lithium fluoride (LiF), and typical scanning electron microscopy (SEM) and transmission electron microscopy (TEM) micrographs of $Ti_3C_2T_x$ MXene flakes were provided in Fig. S1. The as-prepared MXene platelets show obvious layered structure and flat feature, and the interlayer spacing dramatically broadens to be around 2.85 nm after ultrasonic treatment, which is beneficial for charge storage. Fig. 2a shows a digital photograph of the as-fabricated paper-based FMSC devices, which can be massively manufactured, including the single, two series, two parallel and four series. The paper-based flexible FMSCs are easy to realize device integration through the design of electrode patterns to meet different needs. The patterned $Ti_3C_2T_x$ MXene paper-based electrodes were imaged by scanning electron microscopy (SEM) (Fig. 2b–c). Due to equipment limitation, the electrode structure has a deviation of about 20 μm. The typical width and distance of the interdigitated electrodes was measured to be around 0.76 mm and 224 μm, respectively. Moreover, the edges of the laser cutting routes are quite smooth, indicating the minor injuries from the UV laser. The detailed surface morphology of the paper electrode was provided in Fig. S2 (Supporting Information), and the few-layer $Ti_3C_2T_x$ MXene sheets can be clearly observed. And the thickness of the MXene layer of the paper-based electrode is around 7.9 μm, determined by the cross-sectional SEM characterization (Fig. 2d).

The crystal structure of $Ti_3C_2T_x$ MXene paper electrode was investigated via X-ray diffraction (XRD), as shown in Fig. 2e. The peak located at about 6.5° assigns to the (002) diffraction plane of MXenes which is associated with the intercalation of a single layer of water molecules between MXene flakes. And another peak appeared at 26° attributes to the paper itself. The XRD results indicate that the $Ti_3C_2T_x$ MXenes are well coated on paper substrate and show no apparently restacked phenomenon. Raman spectroscopy was further used to identify the various chemical and termination species. As shown in Fig. 2f and Table S1 (Supporting Information), the peaks existing in the MXene powder and the MXene coated paper are basically consistent. After etching, MXene was usually terminated by surface functional groups of O, F and OH [26]. Based on previous reports [27,28], the modes at 728 and 584 cm^{-1} come from the vibrations of C atoms in $Ti_3C_2O_2$; and the peaks at 629 and 699 cm^{-1} belong to the vibrations of atoms in $Ti_3C_2(OH)_2$. Herein the terminal groups are heterogeneous as

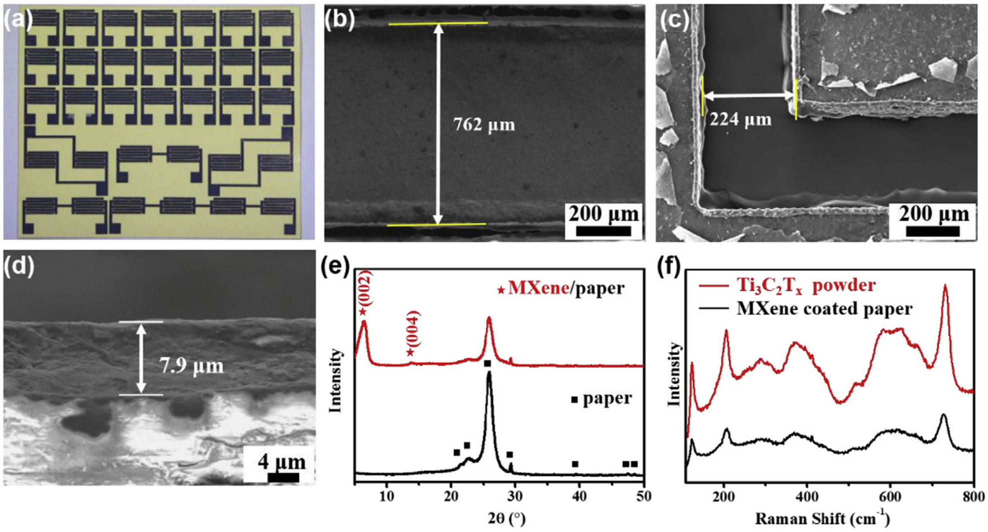

Fig. 2. The detailed processing characterization of as-fabricated FMSCs. (a) Digital photograph showing the massively manufactured paper-based FMSCs (single, two series, two parallel and four series). SEM images showing that (b) the width of the interdigitated electrode was around 0.76 mm; (c) the distance of the interdigitated electrode was around 224 µm. (d) The cross-sectional SEM image of the paper electrode. (e) XRD pattern of $Ti_3C_2T_x$ MXene coated paper electrodes. XRD patterns of blank paper are also given for comparing. (f) Raman spectra of the MXene paper electrode and the freestanding MXene films.

forms of $Ti_3C_2O_2$ and $Ti_3C_2(OH)_2$, which is clearly implied by the bimodal vibration located at around 600 cm^{-1}. A broad peak appeared at about 375 cm^{-1}, which can be attributed to the heterogeneous terminal groups. In fact, the presence of oxygen-containing groups was proved to contributed a lot in capacitance of MXenes [23].

For deep insight into the relationship between the electrochemical performance and the structure of paper-based MXene FMSCs, we have designed paper-based MSCs with different width (*w*) and distance (*d*) of the interdigitated fingers when the finger length is fixed at 10 mm, which are schematically presented as the left part of Fig. 3a. For optimizing the electrochemical properties of interdigitated electrodes, the *d* was varied from 0.2 to 0.7 mm whilst the width kept constant at 2 mm. And the digital photographs of these FMSCs with different distance were shown in Fig. S3 (Supporting Information). Also, the corresponding SEM images were provided to measure the precise *d* values. (Fig. S4, Supporting Information). Further, Fig. 3a shows the mechanism of ionic transport in the paper-based FMSCs with different distance *d*. With the increase of *d* value, the ionic transport pathway gets longer, which hinders the fast ion diffusion and therefore results in deterioration of electrochemical capacitance for the corresponding devices [29]. Fig. 3b shows the cyclic voltammetry (CV) curves of paper-based FMSCs with different distance *d* values at a scan rate of 10 mV s^{-1}. The shapes of all the devices are ideally rectangular, which implies that the electrically ion sorption and the transformation of Ti in different valences can be rapidly established [30]. Moreover, the CVs indicate that the areal capacitance of paper-based FMSCs depends a lot on the *d* values. The device with $d = 0.2$ mm exhibits the highest areal capacitance as the effective area of all these devices keeps constant. In addition, the areal capacitance decreases by 39.3% with increasing the *d* values from 0.2 to 0.7 mm, which can be attributed to that the shortened distance promotes electrolyte-ions transfer, as schematic in Fig. 3a.

The galvanostatic charge-discharge (GCD) testing at the same current density of 0.1 mA cm^{-2} shows the similar results as mentioned above (Fig. 3c). Typical isosceles triangle shapes for the paper-based FMSCs can be observed and the discharge time gets longer as the distance increases. Besides, the minimum voltage drops appeared at the FMSC devices with $d = 0.2$ mm while the maximum voltage drops emerged at $d = 0.7$ mm. The EIS measurement was employed in the frequency range of 100 kHz–100 mHz to further investigate the electrochemical capacitive behavior of the solid-state FMSCs (Fig. 3d). The near vertical straight lines are observed in the low-frequency region, indicating the typical characteristics of capacitive material. As expected, the lowest impedance is obtained in the paper-based FMSC with $d = 0.2$ mm, which can further explain its best capacitive behavior and minimum voltage drops. All above, the distance of the interdigitated fingers plays an essential role in the interdigitated FMSCs, because it can strongly affect the pathway for electrolyte ions transport.

However, typical CV curves of the FMSCs with $d = 0.2$ mm at different scan rates exhibited a good rectangular shape only at low scan rates, as shown in Fig. 3e, which indicates the not perfect rate performance. In addition, Fig. 3f shows the corresponding GCD curves of the FMSCs with isosceles triangle shapes. The corresponding areal capacitance at different current densities was calculated according to Formula 1 (Fig. 3g). As the current density increased from 0.05 to 1 mA cm^{-2}, the areal capacitance decayed from 19.7 to 8.7 mF cm^{-2}, and the capacitance retention is only 44.2%. As mentioned above, despite the FMSCs with $d = 0.2$ mm show the best capacitance performance in this batch of samples, the areal capacitance, voltage drop during charge-discharge, and the rate performance was failed to meet our expectations, which may be caused by the large width of the interdigitated finger. Therefore, to enhance the electrochemical performance of devices, the paper-based FMSCs with different width *w*, stationary distance *d* and length *l* was further investigated.

Fig. 4a shows the digital photograph of the as-fabricated paper-based FMSCs with finger width ranging from 0.5 to 2.5 mm, and a Chinese coin was also placed at the right side for comparison. All these FMSCs possess the same distance around 224 µm, which was measured through the SEM images (Fig. 2c). Fig. 4b–c shows the corresponding CV curves at a scan rate of 10 mV s^{-1} and GCD curves at different current densities, respectively. Since the electrolyte ion can transport to the interior of MXene electrode from both the top side and edge of interdigitated finger, the width plays a key role on ion transport process. On the one side, the paper-based device with $w = 0.8$ mm exhibited the highest areal capacitance which was much higher than that of $w = 1.5$, 2.0, and 2.5 mm, as well as the lowest voltage drop. It's because when the width is in the range of 2.5 to 0.8 mm, the edge side of electrode dominated ion transmission. When the width gets smaller to 0.8 mm, electrolyte ions are easier to enter the electrode interior and the ion transmission path becomes shorter, which ensure the optimal specific capacitance. In addition, the areal capacitance for the FMSCs with $w = 0.5$, 0.8 and 1.0 mm were quite approximative, that is, when the width is less than 1.0 mm, width has little effect on the capacitive performance of interdigitated FMSCs and the areal capacitance tends to be stable. On the other side, when the width increased over than 1.5 mm, the CV curves come close to coinciding in shape (Fig. 4b), indicating that the top side of the finger but not the edge part predominated in the ion transmission. The difference is that the FMSCs with smaller width possess the better charge-discharge efficiency (Fig. 4c). The reason is that the shorter ion transfer distance with the

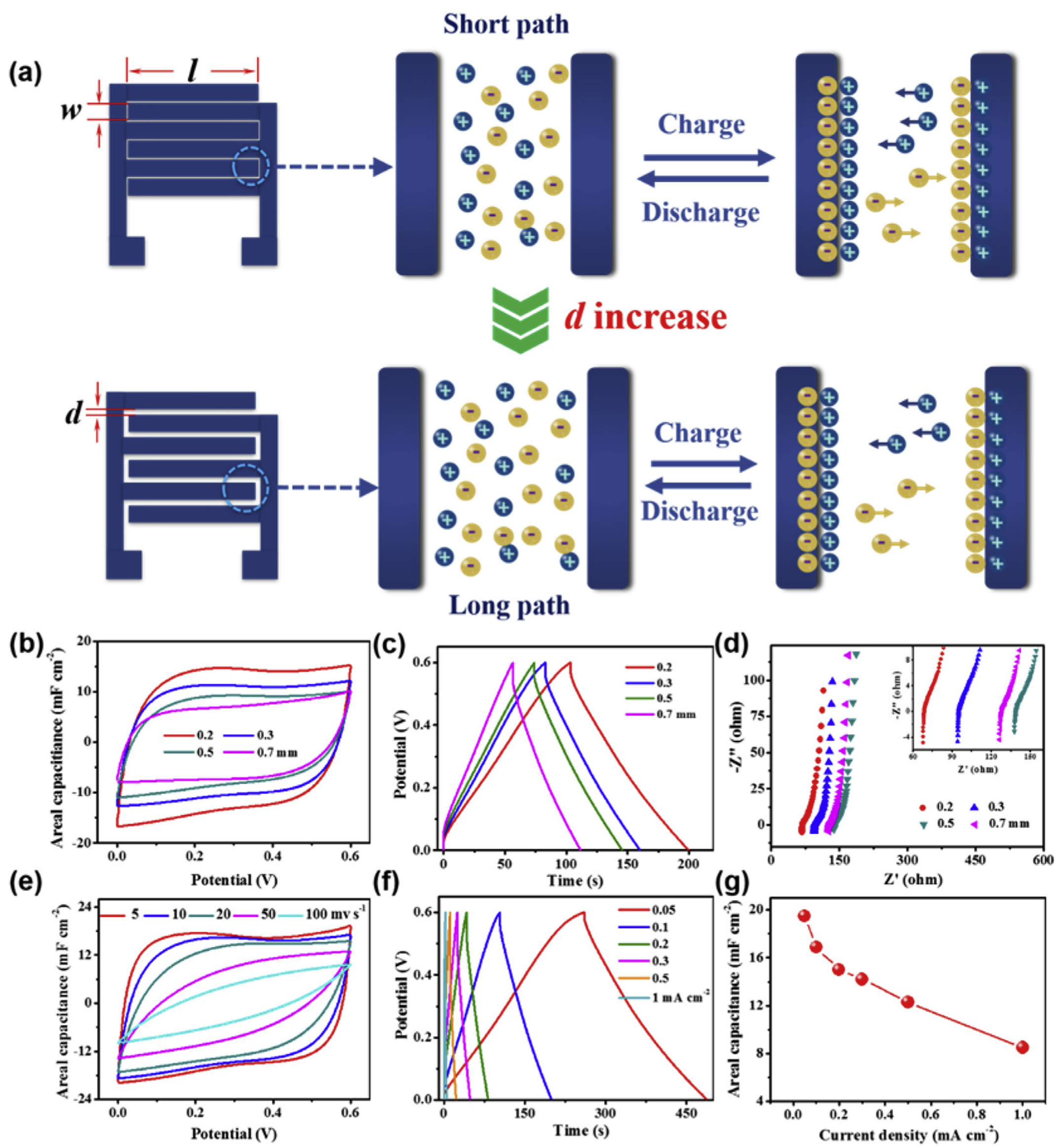

Fig. 3. Electrochemical performance of paper-based FMSCs with different distance ranging from 0.2 to 0.7 mm. (a) Schematic diagram of ion transport mechanism of paper-based FMSCs with different interspaces; (b) CVs at a scan rate of 10 mV s^{-1} of various FMSCs; (c) GCD curves of the FMSCs at a current density of 0.1 mA cm^{-2}; (d) The Nyquist plots for paper-based FMSCs; (e) CVs of the FMSCs with d = 0.2 mm at different scan rates; (f) GCD curves of the FMSCs at different current densities; (g) The variation of areal capacitances for FMSCs with d = 0.2 mm.

decrease of the width, lowering the internal resistance of FMSCs.

The EIS Nyquist plot of these devices is given in Fig. 4d, and the fitted equivalent circuit for the Nyquist plot is present as an insert image. The fitted circuit diagram is composed of equivalent elements including the ohm resistance (Ro), the charge transfer resistance (Rct), the constant phase element (CPE) and the Warburg diffusion element (Wo). In the high-frequency region, increasing Ro values can be observed with the decrease of width, which can be attributed to the decrease of the active area [29]. And in the low-frequency region, the lines are near vertical straight, indicating the typical characters of capacitive material.

Typical CV curves of the FMSCs with w = 0.8 mm, d = 0.2 mm at different scans were shown in Fig. 4e. The geometrically optimized devices exhibit much better electrochemical performance including the areal capacitance and rate-capability. Amazingly, calculated through the GCD curves (Fig. S5, Supporting Information), the optimized FMSCs possess an areal capacitance of 23.4 mF cm^{-2} at 0.05 mA cm^{-2}, and 81.6% (19.2 mF cm^{-2}) capacitance retention at 1 mA cm^{-2} (Fig. 4f). In addition, energy density and power density are also critical parameters for paper-based flexible solid-state FMSCs. From Fig. 4g, the highest volumetric energy densities reach up to 1.48 mWh cm^{-3} at a power density of 189.9 mW cm^{-3}, which are substantially higher than other micro-supercapacitors based on graphene/PANI (0.32 mWh cm^{-3} at 54 mW cm^{-3}) [31], VN/CNT (0.54 mWh cm^{-3} at 400 mW cm^{-3}) [32], rGO-CNT (0.68 mWh cm^{-3} at 77 W cm^{-3}) [33], and PPy-coated paper (1 mWh cm^{-3} at 270 mW cm^{-3}) [34]. Moreover, a high value of 92.4% capacitance retention was remained over 5000 cycles at a GCD current density of 1 mA cm^{-2} (Fig. 4h). The capacitance decay might be attributed to the irreversible oxidization of MXene in aqueous electrolytes with oxygen and positive potentials [30].

To meet the requirements of FMSCs integrated into portable and on-chip microelectronics, the bendable property of paper-based FMSCs is significant for practical applications. Fig. 5a shows the digital images of the device subjected to different bendable states with the bending angle ranging from 0 to 180ºusing the capton glue to fix the devices. Fig. 5b–c shows the CV curves and corresponding capacitance retention ratio of the device at different bending angles. There is no capacitance degradation undergoing different bending loads, obviously indicating

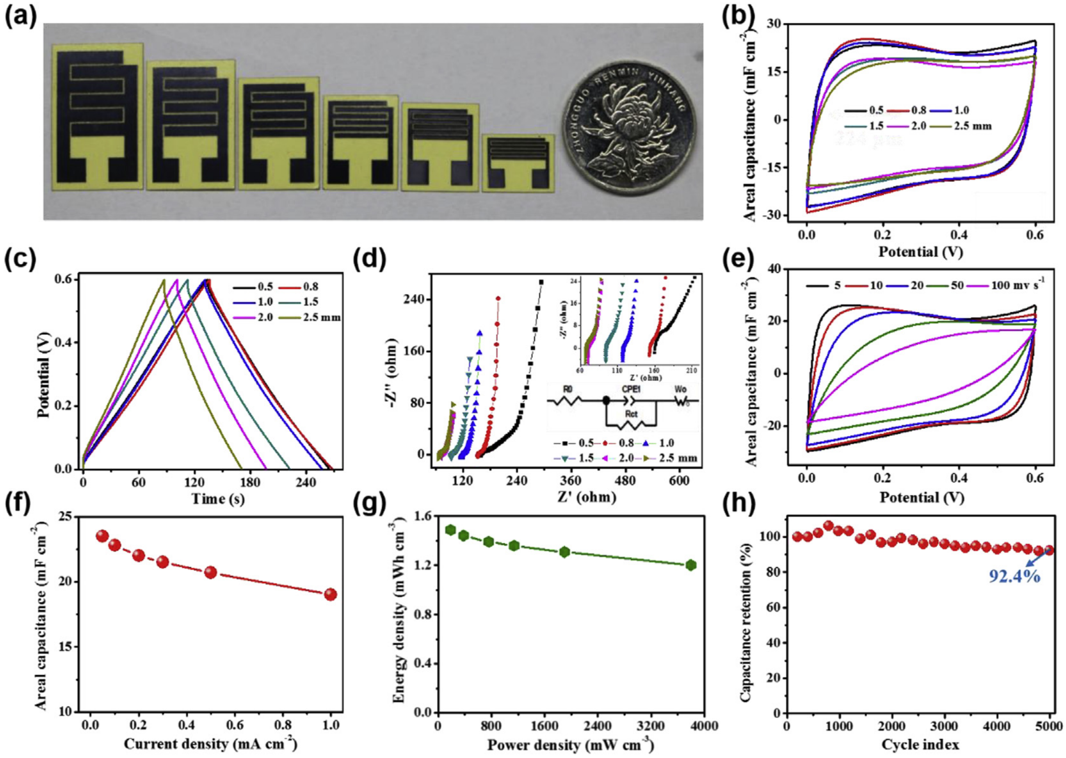

Fig. 4. Electrochemical performance of paper-based FMSCs with different width. (a) Digital photograph of paper-based FMSCs with the finger width ranging from 0.5 to 2.5 mm. A Chinese coin was placed at the right side for size comparison; (b) CVs at a scan rate of 10 mV s^{-1} of various FMSC devices; (c) GCD curves of the FMSCs at the current density of 0.1 mA cm^{-2}; (d) the Nyquist plots for the five paper-based FMSCs. Inset images: the magnified high-frequency region of the Nyquist plot (top) and the equivalent circuit for the Nyquist plot (bottom); (e) CVs of the FMSC devices with w = 0.8 mm at different scan rate; (f) The variation of areal capacitances of the devices with w = 0.8 mm; (g) The Ragone plots for the device of w = 0.8 mm. (h) The cycling performance of the paper-based FMSCs.

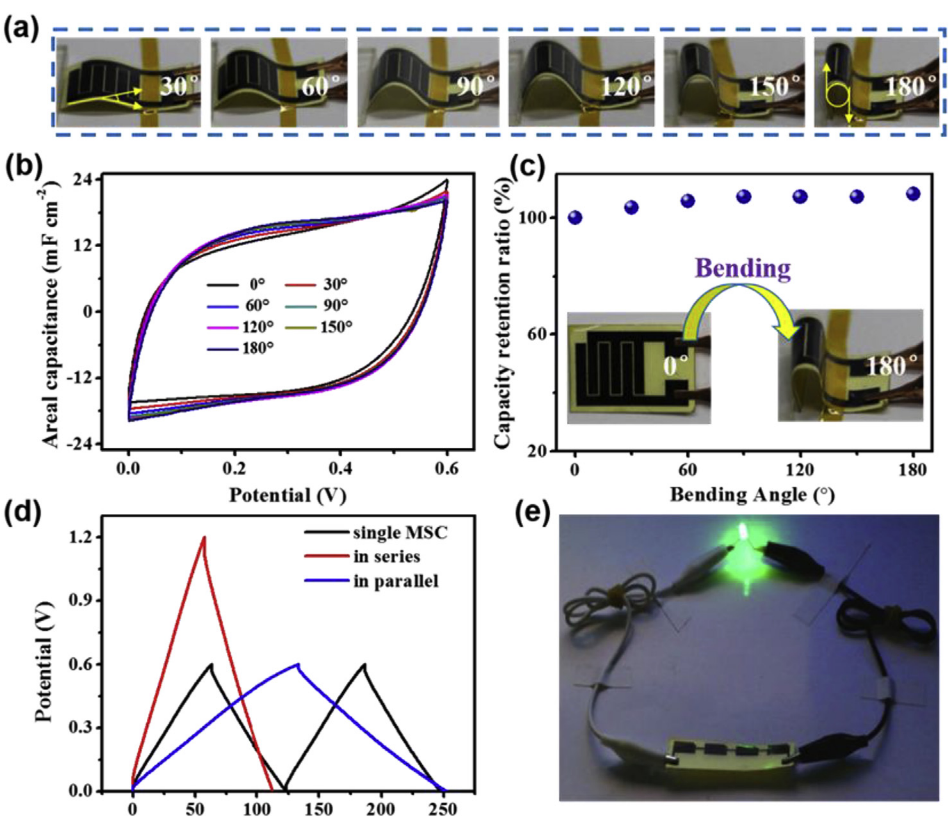

Fig. 5. The flexibility and integration characterization of FMSCs. (a) Digital photograph of paper-based FMSCs with different bending angles; (b) The corresponding CVs at different bending angles; (c) the capacitance retention with bending; (d) GCD curves of the single, two-series, and two-parallel FMSCs; (e) Digital photograph shows the LED lighted by a four-series FMSCs.

excellent flexibility of paper-based FMSCs. Practically, the FMSCs must be connected in parallel and series to obtain the required capacitance and voltage. And these paper-based FMSCs are easy to connect in parallel and series via a one-step laser cutting process, as shown in Fig. S6 (Supporting Information). The paper-based FMSCs in parallel and series were charge-discharged at the current density of $0.2\,mA\,cm^{-2}$ (Fig. 5c). Two FMSCs in series shows the intentional voltage window up to 1.2 V. However, discharge time of two-series device was 8% shorter than that of the single one, which indicates the uniformity of paper electrodes and the performance of FMSC devices can be further optimized. When FMSCs were designed in parallel, the discharge time measured at the same current density increases by 100% for parallel device than a single one, indicating that the desired capacitance can also be realized through device designing. As expected, four paper-based FMSCs connected in serial can support a light-emitting diode (LED) work (Fig. 5e). These results unambiguously demonstrate that paper-based FMSCs illustrate excellent mechanical flexibility, electrochemical properties, and potential application for power and energy supply.

4. Conclusion

In summary, this work presents a simple and feasible method for designing paper-based all-solid-state FMSCs through direct spray coating of conductive MXene inks, which can be further extended to the large family of MXenes and their heterostructures. We prove that geometrical configuration of interdigitated FMSCs plays a key role on the electrochemical properties, as indicated by the smaller width the higher capacitance, and the shorter distance the higher capacitance. As the width and distance decrease to 0.8 mm and 0.2 mm, respectively, the devices show the highest areal capacitances of $23.4\,mF\,cm^{-2}$ at $0.05\,mA\,cm^{-2}$, good rate-capability and excellent cycling stability with over 92.4% capacitance retention after 5000 cycles, along with remarkable flexibility and highly integrated ability. Thus, incorporation of a simple method to massively manufacture paper-based all-solid-state FMSCs with both extraordinary mechanical flexibility and electrochemical performance will make it easier to realize the integration of FMSCs and thus promote their practical application in portable and on-chip microelectronics.

Acknowledgements

We are thankful to Analytical and Testing Center of Southwest Jiaotong University for supporting the SEM measurements. This work was financially supported by the National Natural Science Foundation of China (No. 51602265), the scientific and technological projects for International Cooperation of Sichuan Province (No. 2017HH0069), Special Fund of China Postdoctoral Science Foundation (2018T110992), the Independent Research Project of State Key Laboratory of Traction Power (Nos. 2017TPL_Z04 and 2016TPL_Z03), and the Fundamental Research Funds for the Central Universities of China.

Appendix A. Supplementary data

Supplementary data to this article can be found online at https://doi.org/10.1016/j.jpowsour.2019.01.044.

References

[1] C. Yan, W. Deng, L. Jin, T. Yang, Z. Wang, X. Chu, H. Su, J. Chen, W. Yang, ACS Appl. Mater. Interfaces 10 (2018) 41070–41075.
[2] L. Feng, K. Wang, X. Zhang, X. Sun, C. Li, X. Ge, Y. Ma, Adv. Funct. Mater. 28 (2018) 1704463.
[3] H. Zhang, H. Su, L. Zhang, B. Zhang, F. Chun, X. Chu, W. He, W. Yang, J. Power Sources 331 (2016) 332–339.
[4] H. Li, J. Song, L. Wang, X. Feng, R. Liu, W. Zeng, Z. Huang, Y. Ma, L. Wang, Nanoscale 9 (2016) 193–200.
[5] X.C. Dong, H. Xu, X.W. Wang, Y.X. Huang, M.B. Chanpark, H. Zhang, L.H. Wang, W. Huang, P. Chen, ACS Nano 6 (2012) 3206–3213.
[6] X. Chu, H. Zhang, H. Su, F. Liu, B. Gu, H. Huang, H. Zhang, W. Deng, X. Zheng, W. Yang, Chem. Eng. J. 349 (2018) 168–175.
[7] L. Liu, D. Ye, Y. Yu, L. Liu, Y. Wu, Carbon 111 (2017) 121–127.
[8] Z.-K. Wu, Z. Lin, L. Li, B. Song, K.-s. Moon, S.-L. Bai, C.-P. Wong, Nano Energy 10 (2014) 222–228.
[9] B. Shen, R. Guo, J. Lang, L. Liu, L. Liu, X. Yan, J. Mater. Chem. 4 (2016) 8316–8327.
[10] L. Liu, B. Shen, D. Jiang, R. Guo, L. Kong, X. Yan, Adv. Energy Mater. 6 (2016) 1600763.
[11] D. Kim, J. Yun, G. Lee, J.S. Ha, Nanoscale 6 (2014) 12034–12041.
[12] C.J. Zhang, M.P. Kremer, A. Seral-Ascaso, S.-H. Park, N. McEvoy, B. Anasori, Y. Gogotsi, V. Nicolosi, Adv. Funct. Mater. 28 (2018) 1705506.
[13] Y.Z. Zhang, Y. Wang, T. Cheng, W.Y. Lai, H. Pang, W. Huang, Chem. Soc. Rev. 44 (2015) 5181–5199.
[14] Z.S. Wu, K. Parvez, X. Feng, K. Mullen, Nat. Commun. 4 (2013) 2487.
[15] W. Si, C. Yan, Y. Chen, S. Oswald, L. Han, O.G. Schmidt, Energy Environ. Sci. 6 (2013) 3218.
[16] M. Naguib, V.N. Mochalin, M.W. Barsoum, Y. Gogotsi, Adv. Mater. 26 (2014) 992–1005.
[17] J.-C. Lei, X. Zhang, Z. Zhou, Front. Physiol. 10 (2015) 276–286.
[18] Z. Ling, C.E. Ren, M.Q. Zhao, J. Yang, J.M. Giammarco, J. Qiu, M.W. Barsoum, Y. Gogotsi, Proc. Natl. Acad. Sci. Unit. States Am. 111 (2014) 16676–16681.
[19] D.N. Futaba, K. Hata, T. Yamada, T. Hiraoka, Y. Hayamizu, Y. Kakudate, O. Tanaike, H. Hatori, M. Yumura, S. Iijima, Nat. Mater. 5 (2006) 987–994.
[20] H. Su, H. Huang, H. Zhang, X. Chu, B. Zhang, B. Gu, X. Zheng, S. Wu, W. He, C. Yan, J. Chen, W. Yang, ACS Appl. Energy Mater. 1 (2018) 3544–3553.
[21] S. Wang, N. Liu, J. Su, L. Li, F. Long, Z. Zou, X. Jiang, Y. Gao, ACS Nano 11 (2017) 2066–2074.
[22] Y. Li, G. Wang, T. Wei, Z. Fan, P. Yan, Nano Energy 19 (2016) 165–175.
[23] Y.-Y. Peng, B. Akuzum, N. Kurra, M.-Q. Zhao, M. Alhabeb, B. Anasori, E.C. Kumbur, H.N. Alshareef, M.-D. Ger, Y. Gogotsi, Energy Environ. Sci. 9 (2016) 2847–2854.
[24] S. Kim, T.G. Yun, C. Kang, M.-J. Son, J.-G. Kang, I.-H. Kim, H.-J. Lee, C.-H. An, B. Hwang, Mater. Des. 151 (2018) 1–7.
[25] R. Guo, J. Chen, B. Yang, L. Liu, L. Su, B. Shen, X. Yan, Adv. Funct. Mater. 27 (2017) 1702394.
[26] M. Hu, T. Hu, Z. Li, Y. Yang, R. Cheng, J. Yang, C. Cui, X. Wang, ACS Nano 12 (2018) 3578–3586.
[27] M. Hu, Z. Li, T. Hu, S. Zhu, C. Zhang, X. Wang, ACS Nano 10 (2016) 11344–11350.
[28] G. Fan, X. Li, C. Xu, W. Jiang, Y. Zhang, D. Gao, J. Bi, Y. Wang, Nanomater. (Basel) (2018) 8.
[29] D. Pech, M. Brunet, T.M. Dinh, K. Armstrong, J. Gaudet, D. Guay, J. Power Sources 230 (2013) 230–235.
[30] H. Li, Y. Hou, F. Wang, M.R. Lohe, X. Zhuang, L. Niu, X. Feng, Adv. Energy Mater. 7 (2017) 1601847.
[31] B. Yao, L. Yuan, X. Xiao, J. Zhang, Y. Qi, J. Zhou, J. Zhou, B. Hu, W. Chen, Nano Energy 2 (2013) 1071–1078.
[32] X. Xiao, X. Peng, H. Jin, T. Li, C. Zhang, B. Gao, B. Hu, K. Huo, J. Zhou, Adv. Mater. 25 (2013) 5091–5097.
[33] M. Beidaghi, C. Wang, Adv. Funct. Mater. 22 (2012) 4501–4510.
[34] L. Yuan, B. Yao, B. Hu, K. Huo, W. Chen, J. Zhou, Energy Environ. Sci. 6 (2013) 470.
[35] H. Huang, H. Su, H. Zhang, L. Xu, X. Chu, C. Hu, H. Liu, N. Chen, F. Liu, W. Deng, B. Gu, H. Zhang, W. Yang, Adv. Electron. Mater. 4 (2018) 1800179.